Society of Medical Education & Research

2023, Volume 3, Issue 1, Page No: 116-138

ISSN: 3108-4834

Archive of International Journal of Cancer and Allied Science

Long Noncoding RNAs as Predictive Biomarkers of Peritoneal Recurrence in Gastric Cancer

Oliver Peter Smith[1], Emily Jane Brown[1]*, George Henry Jones[2], Jessica Lynn Williams[2], Charles Edward Davis[3], Megan Rose Taylor[3]

[1]Department of Oncology, Massachusetts General Hospital (MGH), Boston, United States.
[2]Dana-Farber Cancer Institute, Harvard Medical School, Boston, United States.
[3]Memorial Sloan Kettering Cancer Center (MSKCC), New York, United States.

***E-mail** ✉ e.brown.mgh@gmail.com

Abstract

Emerging evidence indicates that long noncoding RNAs (lncRNAs) are deeply involved in the biological processes driving gastric cancer (GC) progression and metastatic spread. Despite this, the prognostic value of tissue-based lncRNA expression for anticipating peritoneal recurrence in GC has not been thoroughly investigated. In the present study, we perform a comprehensive analysis of lncRNA expression patterns associated with peritoneal metastasis (PM) in GC and construct a composite lncRNA-derived risk score to stratify patients according to their likelihood of developing peritoneal recurrence after curative gastrectomy. Transcriptome-wide profiling of long noncoding RNAs was performed on matched peritoneal lesions, primary gastric tumors, and adjacent normal tissues obtained from 12 patients with gastric cancer in the Sun Yat-sen University Cancer Center (SYSUCC) discovery cohort. Candidate lncRNAs were subsequently screened through integrative analyses incorporating data from The Cancer Genome Atlas (TCGA) and an independent SYSUCC validation cohort. An lncRNA-based predictive score was developed using least absolute shrinkage and selection operator (LASSO) modeling combined with Cox regression–derived nomograms, and its performance was assessed by receiver operating characteristic (ROC) analysis. Finally, the functional involvement of selected lncRNAs in gastric cancer peritoneal metastasis was evaluated using wound-healing assays, Transwell migration and invasion assays, three-dimensional multicellular tumor spheroid invasion models, and in vivo peritoneal xenograft mouse models.Five key lncRNAs were identified and integrated into a peritoneal metastasis (PM) risk model for estimating peritoneal recurrence–free survival (pRFS). Building upon this model, we constructed a multidimensional nomogram incorporating the PM risk score alongside pathological T stage, pathological N stage, and tumor size, which demonstrated strong predictive performance for 5-year pRFS (AUC = 0.79, 95% CI: 0.71–0.88). Functional investigations further revealed that CASC15, one of the identified lncRNAs, enhanced gastric cancer cell migratory and invasive capacities in vitro and significantly promoted peritoneal dissemination in vivo, providing initial evidence for the involvement of lncRNAs in GC peritoneal metastasis. Mechanistic studies indicated that CASC15 drives epithelial–mesenchymal transition and metastatic behavior through activation of the JNK and p38 signaling pathways. In this work, we established a clinically applicable composite scoring system based on lncRNA expression to estimate the risk of peritoneal recurrence in patients with gastric cancer.

Keywords: Transcriptome profiles, Gastric cancer, Peritoneal recurrence, Long noncoding RNA

Access this article online https://smerpub.com/

Received: 29 January 2023; **Accepted:** 18 April 2023

How to cite this article: Smith OP, Brown EJ, Jones GH, Williams JL, Davis CE, Taylor MR. Evaluation of Sexual Satisfaction in Pregnant Women with Vaginal Candidiasis. Arch Int J Cancer Allied Sci. 2023;3(1):116-38. https://doi.org/10.51847/6pDQswnKMu

Introduction

Gastric cancer (GC) remains one of the most frequently diagnosed malignancies worldwide, ranking fourth in global incidence, and is commonly diagnosed at an advanced stage due to the absence of distinctive early clinical manifestations, resulting in substantial morbidity and mortality [1, 2]. Among the various metastatic

patterns of GC, the peritoneum is the most frequent site of distant spread and postoperative relapse, emphasizing its significance in disease management [2–4]. Once peritoneal metastasis (PM) develops, patient outcomes are extremely poor, with median survival durations rarely exceeding six months [5]. Therefore, reliable identification of patients at risk for PM is essential for improving clinical decision-making.

Current diagnostic approaches for PM in GC rely primarily on imaging techniques such as computed tomography (CT) and positron emission tomography (PET) [6, 7]. However, both modalities exhibit limited diagnostic performance, particularly for detecting early or occult peritoneal disease [6, 8, 9]. Although laparoscopic staging with histopathological confirmation is regarded as the diagnostic reference standard [7], its invasive nature and limited applicability preclude its routine use in all patients. These limitations underscore the urgent need for noninvasive or minimally invasive biomarkers capable of accurately predicting peritoneal dissemination.

Long noncoding RNAs (lncRNAs), transcripts exceeding 200 nucleotides in length, have emerged as critical regulators of cellular homeostasis through their involvement in epigenetic modulation, transcriptional control, and post-transcriptional regulation [10, 11]. Notably, the expression of many lncRNAs is highly tissue- and context-specific, rendering them attractive candidates for disease-specific biomarker development [12]. Prior studies have demonstrated the clinical relevance of lncRNAs in cancer detection and progression. For example, Liu *et al*. identified tumor-specific lncRNA signatures in esophageal squamous cell carcinoma (ESCC) with potential application in early diagnosis [13]. In gastric cancer, accumulating evidence suggests a strong association between lncRNAs and peritoneal dissemination. Zhou *et al*. reported that lnc-TRIM28-14 expression is markedly elevated in GC patients with PM and improves diagnostic discrimination [14]. Similarly, Zhao *et al*. demonstrated that nanoparticle-mediated delivery of LINC00589 effectively suppressed PM in GC models [15]. Despite these advances, a systematic evaluation of tissue-derived lncRNAs for predicting peritoneal recurrence following curative surgery in GC has not yet been conducted.

To address this gap, the present study comprehensively profiled lncRNA expression across matched peritoneal metastases, primary gastric tumors, and adjacent nonmalignant tissues from 12 patients with GC. By integrating these data with large-scale datasets from The Cancer Genome Atlas (TCGA) and an independent Sun Yat-sen University Cancer Center (SYSUCC) validation cohort, five prognostically relevant lncRNAs were identified. These lncRNAs were subsequently used to construct a peritoneal metastasis risk score capable of stratifying patients according to peritoneal recurrence-free survival (pRFS), with increasing scores indicating elevated recurrence risk. In addition, a multivariable nomogram incorporating the lncRNA-based risk score, pathological T stage, pathological N stage, and tumor size was developed, demonstrating strong predictive value for pRFS, recurrence-free survival (RFS), and overall survival (OS), as well as potential utility in identifying patients likely to benefit from adjuvant chemotherapy. Functional investigations focusing on a representative lncRNA, CASC15, revealed that its overexpression enhanced migratory and invasive behavior of gastric cancer cells in vitro and promoted peritoneal dissemination in vivo, providing mechanistic support for the involvement of lncRNAs in GC peritoneal metastasis. Collectively, this study presents a novel lncRNA-based integrated scoring framework with potential clinical application for individualized prediction of peritoneal recurrence in patients with gastric cancer.

Materials and Methods

Preparation and collection of patient specimens

This investigation was performed in compliance with the principles of the Declaration of Helsinki and received ethical approval from the Institutional Review Board of Sun Yat-Sen University Cancer Center (SYSUCC, Guangzhou, China; IRB No. G2021-036). For transcriptomic analysis, matched samples of nonmalignant gastric tissue, primary gastric tumors, and peritoneal metastases were obtained from 12 patients with gastric cancer (GC) and confirmed peritoneal involvement treated at SYSUCC. These patients underwent palliative gastrectomy due to complications such as tumor-associated bleeding or intestinal obstruction.

An independent validation cohort consisted of 231 patients with pathologically confirmed stage II or III GC who underwent curative gastrectomy at SYSUCC between December 2013 and December 2016, without receiving neoadjuvant chemotherapy or radiotherapy. Eligibility criteria for this cohort included an age of 18

years or older, no restriction on sex, an expected survival of at least three months, and sufficient follow-up duration. Individuals with a prior history of other malignancies within the preceding five years were excluded. Tumor specimens were collected in a freshly frozen state from all enrolled patients. Clinical and pathological information was obtained through retrospective examination of electronic medical records, while long-term outcome data were provided by the institutional follow-up unit. All participants provided written informed consent before enrollment in the study.

lncRNA expression mining and high-throughput data processing

High-throughput RNA sequencing of gastric cancer patients with peritoneal metastasis treated at SYSUCC was performed on the Illumina HiSeq 4000 platform (Illumina, Inc., San Diego, CA, USA). In addition, normalized RNA-seq datasets from gastric carcinoma samples in the TCGA cohort were retrieved via the UCSC Xena data portal (http://xena.ucsc.edu/). Gene expression abundance was subsequently normalized and expressed as transcripts per million (TPM) for downstream analyses.

PM risk score establishment and LASSO regression analysis

To develop a peritoneal metastasis (PM) risk score and select lncRNAs with predictive relevance, we employed LASSO regression. This approach applies an L1 penalty that eliminates less significant variables by reducing their coefficients to zero. The penalty intensity is determined by the tuning parameter λ, which we gradually lowered to allow additional lncRNAs into the model. To identify the optimal λ, we performed 200-fold cross-validation and selected the value using the 1-standard error (SE) rule. The PM risk score for each patient in the SYSUCC and TCGA cohorts was then calculated using the formula: PM risk score= ∑exp(i) * coef(i), In this formula, exp(i) represents the measured expression level of a given lncRNA, and coef(i) is its coefficient obtained from the LASSO regression, providing a weighted estimate of peritoneal recurrence risk.

Cells culture

Cell lines including AGS, BGC823, GES1, HGC27, MKN28, SNU216, and SNU719 were propagated in either DMEM or RPMI-1640 medium (Invitrogen, Carlsbad, USA) supplemented with 10% fetal bovine serum (FBS; Gibco, NY, USA). The cultures were maintained at 37 °C in a humidified incubator with 5% CO_2, using culture dishes supplied by JET BIOFIL (Guangzhou, China). All cell lines were routinely screened and confirmed to be Mycoplasma-free.

Chemicals and antibodies

This investigation made use of the following antibodies for Western blotting (also referred to as immunoblotting or IB): Dilution 1:2000 — α-Smooth muscle actin (Proteintech 14395), Dilution 1:2000 — Vimentin (Proteintech 60330), Dilution 1:3000 — β-Catenin (Proteintech 51067), Dilution 1:1000 — GAPDH (Proteintech 60004), Dilution 1:1000 — E-Cadherin (BD Biosciences 610182), Dilution 1:1000 — N-Cadherin (BD Biosciences 610921), Dilution 1:1000 — p38 (Cell Signaling Technology (CST) 9212), Dilution 1:1000 — Phospho-p38 (Cell Signaling Technology (CST) 4511), Dilution 1:1000 — JNK (Cell Signaling Technology (CST) 9252), Dilution 1:1000 — Phospho-JNK (Cell Signaling Technology (CST) 9255), Dilution 1:1000 — ERK1/2 (Cell Signaling Technology (CST) 4695), Dilution 1:1000 — Phospho-ERK1/2 (Cell Signaling Technology (CST) 4370),

The small-molecule compounds applied in the experiments were SB203580 (Selleck Chemistry S1076), SP600125 (Selleck Chemistry S1460), and Anisomycin (Selleck Chemistry S7409).

Generation of stable cell lines

Overexpression plasmids for CASC15, along with short hairpin RNA (shRNA) constructs (sequences: sh1 - TTGGCAGTCACACTTGGACTC; sh2 - AAGAAATCAAGCCTGCCCATA), were sourced from TSINGKE (Guangzhou, China). To produce lentiviruses, HEK293T cells were co-transfected with the relevant plasmid together with the packaging vector psPAX2 and the envelope vector pMD2.G, employing JetPrime transfection reagent (Polyplus, France). Lentiviral-containing supernatant was then harvested and applied to infect the desired target cells, achieving stable integration. Following infection, stable cell populations were isolated through puromycin treatment over several days, with knockdown or overexpression levels validated via RT-PCR. For bioluminescence imaging in vivo, a separate transduction was performed using lentiviral vectors encoding Gaussia luciferase (Gluc), after which cells were selected with geneticin.

Quantitative RT-PCR

Total RNA was obtained from cellular or tissue samples via TRIzol extraction (Invitrogen, Carlsbad, CA, USA) and subsequently synthesized into cDNA employing a reverse transcription kit (TAKARA, Beijing, China). Quantitative RT-PCR analysis was performed with SYBR Green SuperMix (Roche, Basel, Switzerland), normalizing data against the GAPDH reference gene.

Western blotting

Cells were lysed on ice for 30 minutes using a lysis buffer composed of 50 mM Tris-HCl (pH 7.4), 150 mM NaCl, 1 mM EDTA, 0.5% NP-40, and 10% glycerol, supplemented with a protease inhibitor cocktail (CW2200S, CWBIO, China). Protein concentrations were measured using a BCA Protein Assay Kit (GLPBIO, GK10009), and samples were denatured at 100 °C for 10 minutes after addition of SDS loading buffer. Proteins were then resolved by SDS-PAGE and transferred onto polyvinylidene fluoride (PVDF) membranes. Following blocking with 5% milk, membranes were incubated with specific primary and secondary antibodies and visualized using the ChemiDoc Touch imaging system (Bio-Rad, USA).

Transwell assays

Cells were prepared in serum-free 1640 medium at densities of 5×10^4 for invasion assays and 2×10^4 for migration assays, and added to the top chamber of 24-well Boyden inserts. Inserts were either coated with Matrigel to evaluate invasive capability or left uncoated for migration analysis (BD Biosciences, New Jersey, USA). The bottom chamber was filled with medium containing 20% serum to act as a chemoattractant. Following a 24-hour incubation period, cells that remained on the upper membrane surface were carefully removed. The cells that had passed through the membrane were fixed in methanol, stained with crystal violet, and subsequently observed and quantified under a microscope.

Wound-healing assay

Gastric cancer cells were evenly plated in 6-well plates and allowed to attach overnight. Once adhered, linear scratches were made across the cell monolayer using a 200-μL pipette tip to simulate wounds. The wells were gently rinsed with PBS to remove detached cells, and serum-free medium was added. Initial images were captured under a microscope to serve as baseline controls. After 24 hours of incubation, the same fields were photographed again to assess cell migration into the wound area.

Cell proliferation detection

Gastric cancer (GC) cells were plated at a density of 2×10^3 cells per well in 96-well plates and maintained under standard culture conditions. Cell proliferation was evaluated at 24-hour intervals using the Cell Counting Kit-8 (CCK-8) assay (MCE, Shanghai, China) in accordance with the manufacturer's protocol.

Colony formation assay

Cells were trypsinized and seeded at 500–1000 cells per well in 6-well plates. Following an initial 24-hour attachment period, cells were grown in either control medium or medium containing the specified compounds for 10–14 days until visible colonies developed. Colonies were then fixed in methanol for 20 minutes at room temperature, stained with 0.5% crystal violet for 2 hours, rinsed, and air-dried. Images of the plates were captured using a ChemiDoc Touch imaging system (Bio-Rad, USA), and colony areas were quantified with ImageJ software.

3D multicellular tumor spheroids invasion assay

Three-dimensional co-culture was carried out as described previously [16]. In brief, 1×10^4 GC cells were suspended in growth medium containing 2% Matrigel and overlaid with additional medium. The culture medium was replaced every 2 days for one week. Bright-field micrographs were obtained with Olympus Cell Sens Standard software (version 1.9), and invasive areas were measured quantitatively.

In-situ hybridization (ISH) staining

A human lncRNA CASC15-specific ISH kit was obtained from Bioster-Bio (Wuhan, China). The ISH procedure was conducted following the manufacturer's guidelines. In short, paraffin-embedded sections were deparaffinized in xylene, rehydrated, and treated with pepsin for antigen retrieval. Sections were then hybridized overnight with digoxin-labeled probes, followed by incubation with streptavidin-horseradish peroxidase and color development using 3,3′-diaminobenzidine (DAB) for visualization.

Fluorescence in-situ hybridization (FISH) and phalloidin staining

A CY3-conjugated CASC15 FISH probe was custom-synthesized by TSINGKE (Guangzhou, China). FISH was performed using the RNA FISH Kit (GenePharma, China) according to the supplied protocol. For actin cytoskeleton visualization, cells were grown on confocal dishes, fixed in 4% paraformaldehyde, permeabilized with 0.5% Triton X-100, and incubated with phalloidin for 20 minutes. Nuclear counterstaining was achieved with 4′,6-diamidino-2-phenylindole (DAPI). Fluorescent images were collected on an Olympus FV1000 confocal microscope (Tokyo, Japan).

Xenograft tumorigenicity assay in mice

Female NSG or BALB/c nude mice aged five weeks (Vital River Laboratory Animal Technology, Beijing, China) were randomly assigned to two or three groups. For intraperitoneal injection in BALB/c nude mice, 1×10^7 AGS cells or 6×10^6 SNU719 cells were resuspended in 100 µL sterile PBS containing 20% high-concentration Matrigel (CORNING, NY, USA). In NSG mice, 5×10^6 MKN28 cells were administered similarly. At designated intervals, 150 µL of 15 mg/mL D-luciferin (GoldBio, cat. no. LUCK-1) was intraperitoneally injected to enable bioluminescent imaging of tumors using the Xenogen IVIS Lumina Series II system. Animals were humanely euthanized 4 weeks post-injection.

Statistical analysis

Where applicable, continuous data were analyzed using unpaired two-tailed Student's t-tests or Mann-Whitney U tests. Categorical data were assessed with χ^2 tests or Fisher's exact tests. Relapse-free survival (pRFS and RFS) and overall survival (OS) curves were generated via the Kaplan-Meier method with log-rank testing, while hazard ratios (HR) were derived from Cox proportional hazards regression. Analyses were performed in R software (version 4.3.2). LASSO regression utilized the "glmnet" package, and nomograms were constructed with the "rms" package. Diagnostic accuracy was evaluated through receiver operating characteristic (ROC) curves and area under the curve (AUC) values. Confidence intervals for AUCs were calculated using the "timeROC" package, and survival visualizations employed the "survminer" package. All experimental assays were repeated at least three times, with results shown from a representative replicate. Values are expressed as mean ± standard deviation (S.D.). Differences were considered statistically significant at $P < 0.05$, determined by two-tailed Student's t-test or two-way ANOVA.

Results and Discussion

Profiling lncRNAs in gastric cancer with peritoneal metastasis

To identify lncRNAs associated with peritoneal metastasis (PM) in gastric cancer (GC), we performed a clinical discovery and validation study across multiple platforms **(Figure 1a).** In the discovery cohort from Sun Yat-sen University Cancer Center (SYSUCC), we analyzed paired samples of normal gastric tissue, primary tumors, and peritoneal metastases from 12 GC patients. A heatmap **(Figure 1b)** displays the lncRNAs showing differential expression among these tissue types. Volcano plots further highlighted lncRNAs with significant up- or downregulation between normal tissue and primary tumors **(Figure 1c),** as well as between normal tissue and PM samples **(Figure 1d).**

To focus on lncRNAs with potential prognostic relevance, we examined transcriptomic data from 414 GC patients in the TCGA database, comparing primary tumors with adjacent normal tissue. This analysis yielded 10 candidate lncRNAs **(Figure 1a)** whose expression levels were associated with survival outcomes. Kaplan–Meier analysis in the TCGA cohort revealed that patients with high versus low expression of these lncRNAs had markedly different prognoses **(Figure 1b).** Additionally, the expression patterns of the 10 lncRNAs were evaluated across normal gastric tissue, primary tumors, and PM samples **(Figure 1e).** These findings suggest that the selected lncRNAs may serve as potential biomarkers for predicting both peritoneal metastasis and patient prognosis.

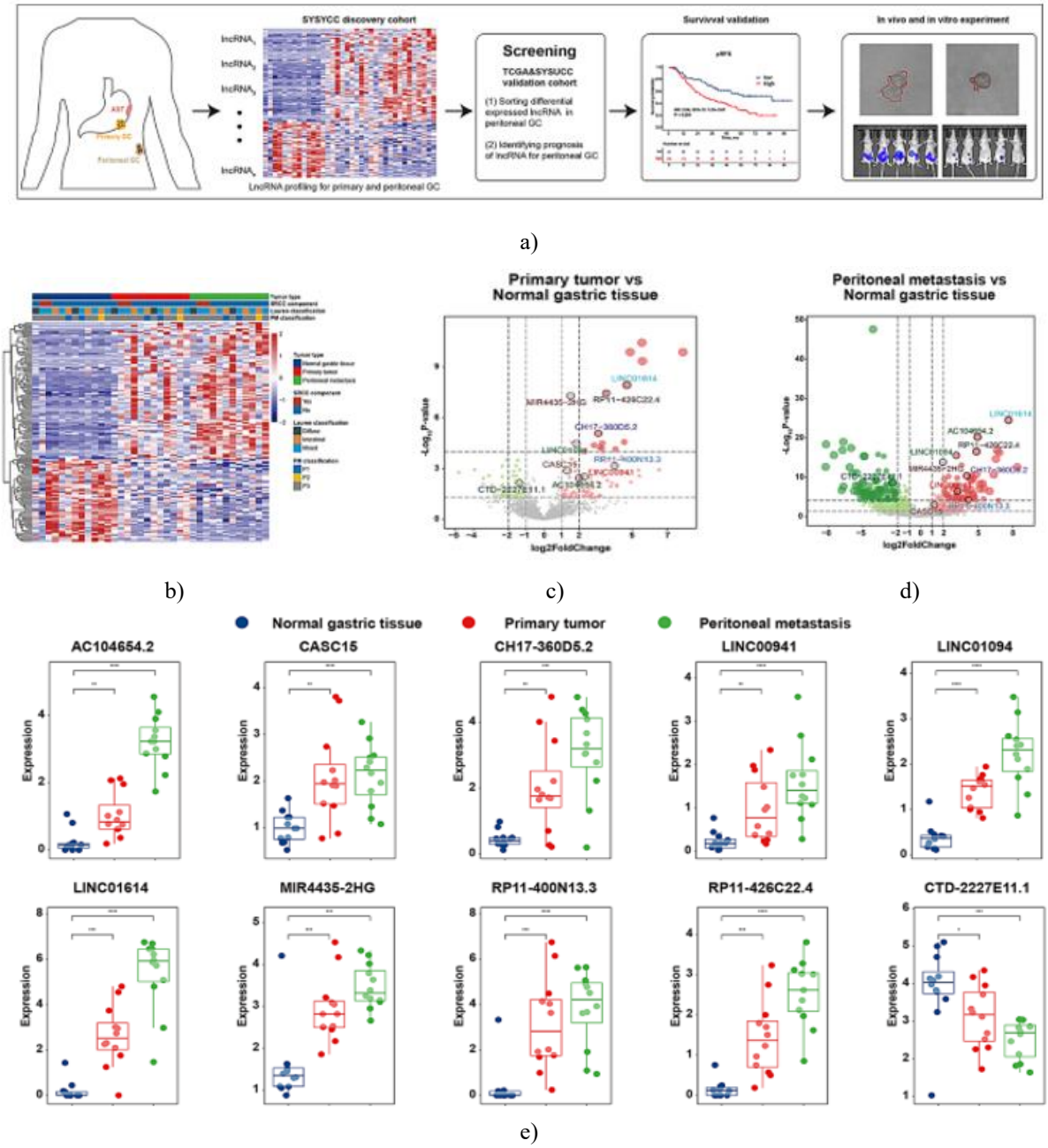

Figure 1. Characterization of long non-coding RNA (lncRNA) expression profiles in gastric cancer patients with peritoneal metastasis.

(a) Schematic overview of the experimental workflow and study design. **(b)** Heatmap illustrating the differentially expressed lncRNAs across matched normal gastric mucosa, primary gastric tumors, and peritoneal metastases in the discovery cohort from Sun Yat-sen University Cancer Center (SYSUCC). **(c)** Volcano plot showing the $\log_2$ (fold change) and statistical significance of lncRNAs differentially expressed between primary gastric tumors and adjacent normal gastric tissues. **(d)** Volcano plot depicting the $\log_2$ (fold change) and significance levels of lncRNAs differentially expressed between peritoneal metastases and normal gastric tissues. **(e)** Box plots displaying the relative expression levels of the top 10 selected lncRNAs in paired samples of normal gastric tissue, primary gastric tumors, and peritoneal metastases. Statistical comparisons were performed

using the Mann-Whitney U test. *P < 0.05, **P < 0.01, ***P < 0.001, ****P < 0.0001.

Abbreviations: ANT, adjacent normal tissues; GC, gastric cancer; lncRNA, long non-coding RNA; PM, peritoneal metastasis; SRCC, signet-ring-cell carcinoma; SYSUCC, Sun Yat-sen University Cancer Center; TCGA, The Cancer Genome Atlas.

Genome-wide identification of lncRNAs linked to peritoneal metastasis

To explore lncRNAs associated with peritoneal recurrence in gastric cancer, we analyzed tissue samples from 231 patients with stage II or III disease who had undergone radical gastrectomy. Total RNA was isolated from these specimens, and the expression of the 10 previously identified lncRNAs was quantified using RT-PCR. Patients were stratified into high- and low-expression groups based on optimal cut-off values. LINC00941 was excluded from further analysis because its expression levels were too low for reliable comparison. Among the remaining nine lncRNAs, elevated levels of seven—AC104654.2, CASC15, CH17-360D5.2, LINC01094, LINC01614, MIR4435-2HG, and RP11-400N13.3—were associated with significantly shorter peritoneal recurrence-free survival (pRFS) **(Figure 2a).** These results were visualized using a forest plot. In addition, the prognostic potential of all nine lncRNAs was evaluated for both recurrence-free survival (RFS) and overall survival (OS) **(Figure 2),** highlighting their potential as predictive biomarkers for GC patients at risk of peritoneal metastasis.

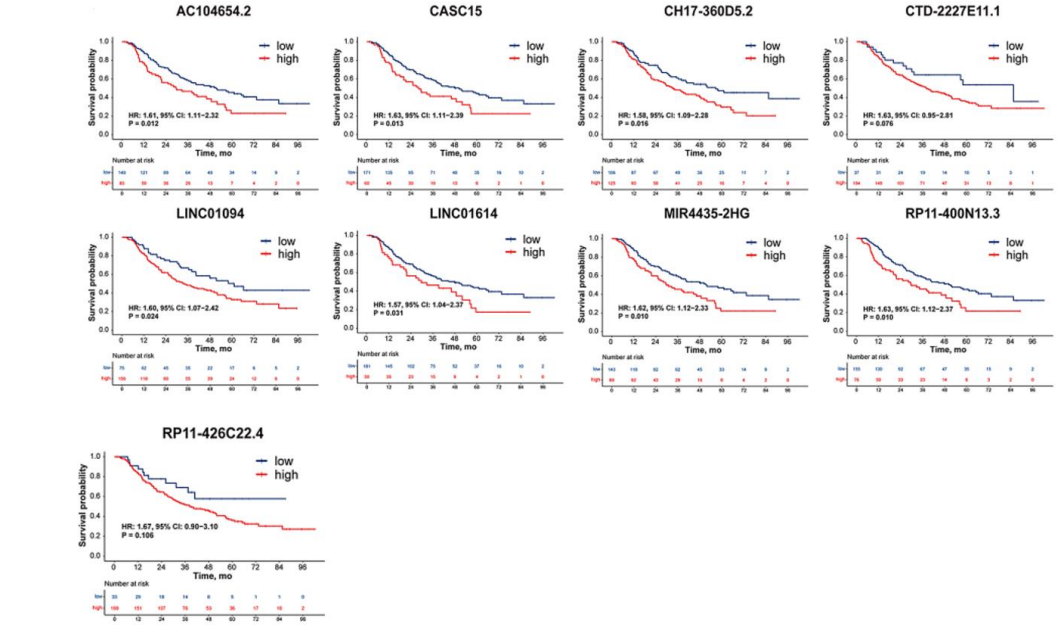

a)

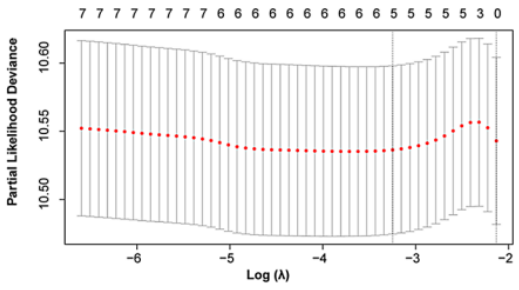

b)

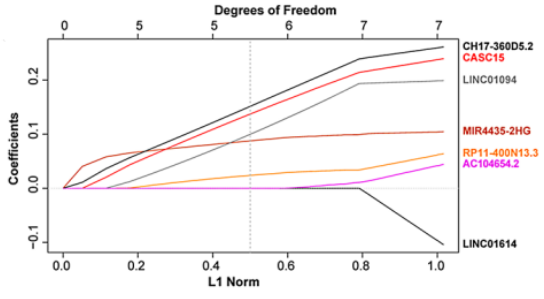

c)

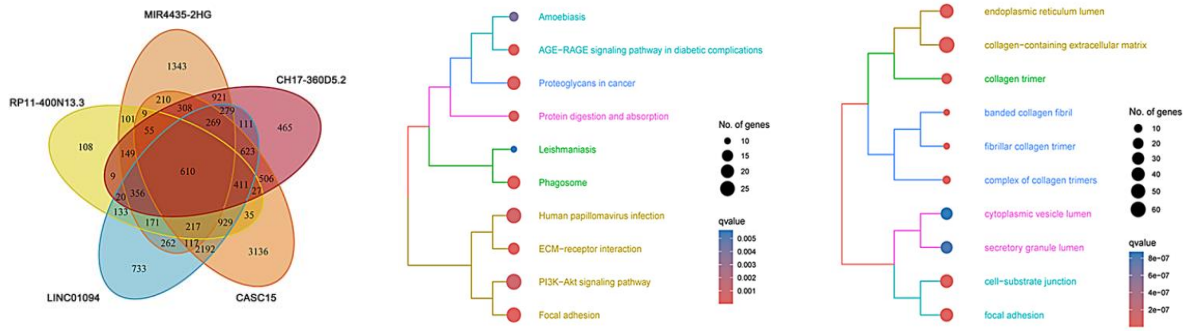

d) e) f)

Figure 2. Broad-scale screening for lncRNAs linked to peritoneal dissemination across the genome.

(a) Survival plots using the Kaplan-Meier method for peritoneal recurrence-free survival (pRFS), comparing patients with elevated versus reduced expression of nine lncRNAs measured by qRT-PCR in the validation set from Sun Yat-sen University Cancer Center (SYSUCC). **(b)** Partial likelihood deviance plot from LASSO regression analysis of seven lncRNAs, with lambda parameter optimized through 200 iterations of cross-validation. **(c)** Trajectories of LASSO coefficients for each lncRNA, illustrated as separate colored lines. **(d)** Venn diagram indicating the overlap of mRNAs showing significant co-expression (Pearson correlation > 0.1) with the five selected lncRNAs in the TCGA dataset. **(e-f)** Results from functional enrichment, covering KEGG pathways (e) and Gene Ontology categories (f) for mRNAs correlated with the five lncRNAs.

Abbreviations: CI, confidence interval; HR, hazard ratio; pRFS, peritoneal recurrence-free survival; SYSUCC, Sun Yat-sen University Cancer Center.

By applying LASSO regression, we pinpointed five lncRNAs—CASC15, CH17-360D5.2, LINC01094, MIR4435-2HG, and RP11-400N13.3—as candidate markers for peritoneal metastasis (PM) risk **(Figure 2b and c)**. Analysis of the TCGA data revealed 610 mRNAs with strong correlations to these lncRNAs **(Figure 2d).** Enrichment studies showed that these correlated mRNAs were primarily associated with well-established oncogenic pathways, including PI3K-Akt signaling, extracellular matrix (ECM)-receptor interactions, focal adhesions, and collagen-rich extracellular matrices **(Figures 2e and f).** Such pathways have been implicated in metastatic progression [17] and alterations in the metastatic niche matrix [18], supporting their role in gastric cancer peritoneal spread and their value for anticipating recurrence at peritoneal sites.

Establishment of a risk score for peritoneal metastasis to forecast recurrence in gastric cancer

In the initial discovery stage, we constructed an integrated PM risk score based on the five identified lncRNAs to estimate the likelihood of peritoneal recurrence. During validation, the PM risk scores and key clinicopathological variables for the 231 cases in the SYSUCC group are depicted in **Figure 3a,** revealing substantially higher scores among patients who developed PM. Cases were divided into high-risk (n=149) and low-risk (n=82) categories. Survival analysis via Kaplan-Meier plots indicated markedly inferior pRFS **(Figure 3b),** RFS **(Figure 3c),** and OS **(Figure 3d)** in the high-risk category, yielding hazard ratios of 2.04 (95% CI: 1.35–3.07; P < 0.001), 1.93 (95% CI: 1.31–2.85; P < 0.001), and 1.83 (95% CI: 1.21–2.76; P = 0.004), respectively. The high-risk group also showed elevated cumulative risks of peritoneal relapse and death **(Figure 3e)**. Validation in the TCGA dataset focused on overall survival (OS) due to incomplete recurrence data; risk scores and clinical features for the 414 TCGA patients are illustrated in **Figure 3f.** High-risk patients displayed reduced OS (**Figure 3g)** with a hazard ratio of 1.82 (95% CI: 1.23–2.68; P = 0.003). These observations aligned closely with SYSUCC findings, confirming the score's reliability in prognosticating gastric cancer outcomes.

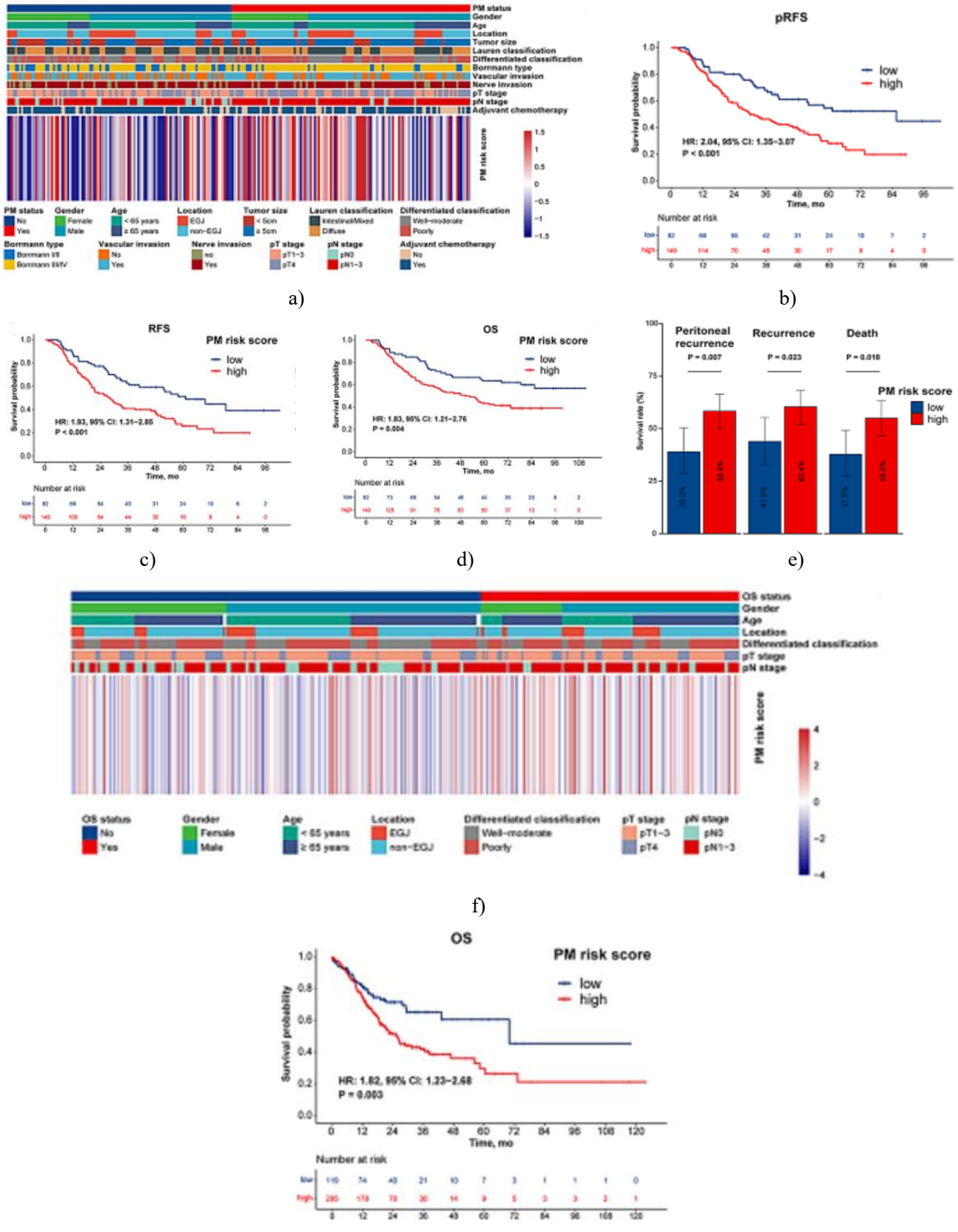

Figure 3. Construction of a risk score for Peritoneal Metastasis (PM) to forecast peritoneal recurrence in gastric cancer

(a) Heatmap illustrating how the PM risk score varies across patients, alongside key clinicopathologic variables, in the validation set from Sun Yat-sen University Cancer Center (SYSUCC). **(b–d)** Kaplan-Meier plots comparing peritoneal recurrence-free survival (pRFS; B), overall recurrence-free survival (RFS; **C),** and overall survival (OS; D) between patients classified as high- or low-risk based on the PM score. **(e)** Box plots highlighting differences in peritoneal recurrence rates, total recurrence rates, and mortality between the high- and low-risk groups. **(f)** Heatmap of PM risk score distribution and related clinicopathologic features in the independent TCGA dataset. **(g)** Kaplan-Meier analysis showing overall survival differences by high versus low PM risk score in the TCGA cohort.

Abbreviations: SYSUCC = Sun Yat-sen University Cancer Center; TCGA = The Cancer Genome Atlas; PM = peritoneal metastasis; EGJ = esophagogastric junction; pRFS = peritoneal recurrence-free survival; RFS = recurrence-free survival; OS = overall survival; HR = hazard ratio; CI = confidence interval.

Combining the risk score with clinical factors enhances prediction of peritoneal recurrence

We conducted univariate and multivariate Cox proportional hazards analyses to identify predictors of pRFS, RFS, and OS within the SYSUCC dataset. According to **Table 1**, the PM risk score, along with tumor size, pathologic T stage, pathologic N stage, and use of adjuvant chemotherapy, were confirmed as independent predictors of pRFS.

To boost predictive power, we built a competing-risk nomogram that incorporated the PM risk score together with tumor size, pT stage, and pN stage **(Figure 4a).** This combined model showed excellent discrimination for pRFS, with a 5-year area under the receiver operating characteristic curve (AUC) of 0.79 (95% CI: 0.71–0.88) **(Figure 4b).**

Patients in the SYSUCC cohort were then reassigned to high-risk (n = 157) or low-risk (n = 74) categories using a composite score derived from the nomogram. The separation in outcomes between these two groups was markedly stronger than that achieved by the PM risk score alone (pRFS: HR 4.57, 95% CI 2.72–7.66, P < 0.001; RFS: HR 3.81, 95% CI 2.38–6.10, P < 0.001; OS: HR 4.50, 95% CI 2.64–7.65, P < 0.001) **(Figure 4c).**

Moreover, at 2-, 3-, and 5-year time points, the composite score provided significantly better prognostic accuracy for pRFS, RFS, and OS than any of the individual components alone (P < 0.05; **Figure 4d**).

Table 1. Results from univariate and multivariate cox regression analyses examining factors associated with peritoneal recurrence-free survival (pRFS), recurrence-free survival (RFS), and overall survival (OS) in the SYSUCC cohort.

Outcome	Variable	Univariate HR (95% CI)	Univariate P-value	Multivariate HR (95% CI)	Multivariate P-value
pRFS	PM risk score (high vs. low)	2.04 (1.35–3.07)	<0.001	1.73 (1.14–2.64)	0.011
	Gender (male vs. female)	1.33 (0.90–1.95)	0.153	—	—
	Age (≥65 vs. <65 years)	1.14 (0.77–1.70)	0.509	—	—
	Tumor location (non-EGJ vs. EGJ)	0.97 (0.67–1.41)	0.882	—	—
	Tumor size (≥5 vs. <5 cm)	2.53 (1.64–3.90)	<0.001	1.87 (1.18–2.95)	0.008
	Borrmann type (III–IV vs. I–II)	2.65 (1.60–4.38)	<0.001	1.60 (0.93–2.75)	0.086
	Differentiation (G3 vs. G1/G2)	1.15 (0.80–1.66)	0.453	—	—
	Lauren type (diffuse vs. intestinal/mixed)	1.08 (0.75–1.55)	0.672	—	—
	Nerve invasion (present vs. absent)	1.47 (0.89–2.42)	0.135	—	—
	Vascular invasion (present vs. absent)	1.52 (1.05–2.19)	0.025	1.18 (0.81–1.72)	0.377
	pT stage (T4 vs. T1–3)	2.16 (1.49–3.13)	<0.001	1.49 (1.01–2.21)	0.045
	pN stage (N1–3 vs. N0)	2.98 (1.45–6.11)	0.003	2.90 (1.39–6.05)	0.005

	Adjuvant chemotherapy (yes vs. no)	0.53 (0.36–0.78)	0.001	0.55 (0.37–0.82)	0.003
RFS	PM risk score (high vs. low)	1.93 (1.31–2.85)	<0.001	1.66 (1.11–2.47)	0.014
	Gender (male vs. female)	1.42 (0.97–2.07)	0.072	—	—
	Age (≥65 vs. <65 years)	1.20 (0.82–1.75)	0.344	—	—
	Tumor location (non-EGJ vs. EGJ)	1.00 (0.70–1.44)	0.989	—	—
	Tumor size (≥5 vs. <5 cm)	2.57 (1.68–3.92)	<0.001	1.90 (1.21–2.97)	0.005
	Borrmann type (III–IV vs. I–II)	2.40 (1.50–3.84)	<0.001	1.49 (0.90–2.46)	0.123
	Differentiation (G3 vs. G1/G2)	1.08 (0.76–1.54)	0.679	—	—
	Lauren type (diffuse vs. intestinal/mixed)	1.00 (0.70–1.42)	0.985	—	—
	Nerve invasion (present vs. absent)	1.35 (0.84–2.18)	0.217	—	—
	Vascular invasion (present vs. absent)	1.52 (1.07–2.17)	0.021	1.23 (0.85–1.77)	0.270
	pT stage (T4 vs. T1–3)	2.10 (1.46–3.00)	<0.001	1.49 (1.02–2.18)	0.039
	pN stage (N1–3 vs. N0)	2.25 (1.21–4.18)	0.010	2.14 (1.13–4.05)	0.019
	Adjuvant chemotherapy (yes vs. no)	0.55 (0.38–0.81)	0.003	0.58 (0.40–0.87)	0.008
OS	PM risk score (high vs. low)	1.83 (1.21–2.76)	0.004	1.57 (1.03–2.41)	0.037
	Gender (male vs. female)	1.26 (0.85–1.87)	0.255	—	—
	Age (≥65 vs. <65 years)	1.23 (0.82–1.84)	0.318	—	—
	Tumor location (non-EGJ vs. EGJ)	0.91 (0.62–1.33)	0.624	—	—
	Tumor size (≥5 vs. <5 cm)	2.55 (1.63–3.97)	<0.001	1.89 (1.17–3.05)	0.009
	Borrmann type (III–IV vs. I–II)	2.51 (1.49–4.20)	<0.001	1.49 (0.86–2.60)	0.158
	Differentiation (G3 vs. G1/G2)	1.15 (0.79–1.66)	0.470	—	—
	Lauren type (diffuse vs. intestinal/mixed)	1.15 (0.79–1.66)	0.467	—	—
	Nerve invasion (present vs. absent)	1.54 (0.91–2.62)	0.109	—	—
	Vascular invasion (present vs. absent)	1.61 (1.10–2.34)	0.013	1.29 (0.88–1.89)	0.188
	pT stage (T4 vs. T1–3)	2.01 (1.38–2.93)	<0.001	1.36 (0.91–2.04)	0.131
	pN stage (N1–3 vs. N0)	3.08 (1.50–6.33)	0.002	2.80 (1.33–5.87)	0.006
	Adjuvant chemotherapy (yes vs. no)	0.46 (0.31–0.69)	<0.001	0.45 (0.30–0.67)	<0.001

pRFS, peritoneal recurrence-free survival; SYSUCC, Sun Yat-Sen University Cancer Center; OS, overall survival; RFS, recurrence-free survival; CI, confidence interval; HR, hazard ratio; EGJ, esophagogastric junction; PM, peritoneal metastasis

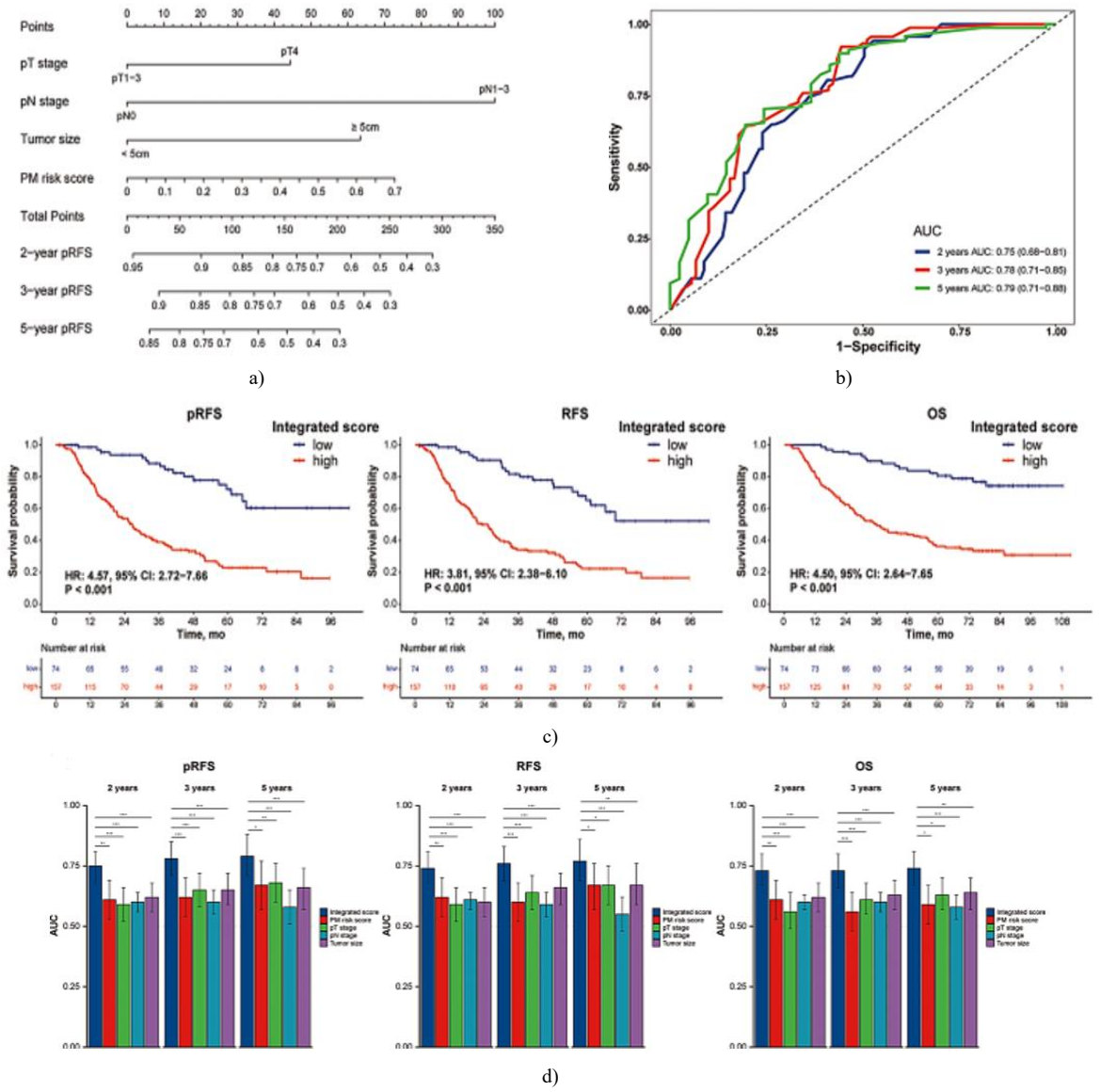

Figure 4. Combined risk score boosts accuracy in forecasting peritoneal recurrence

a. Nomogram for calculating a combined risk score, derived from Cox regression analysis incorporating the peritoneal metastasis (PM) risk score, pathologic T stage, pathologic N stage, and tumor size, in the Sun Yat-sen University Cancer Center (SYSUCC) validation cohort. **b.** Time-dependent receiver operating characteristic (ROC) curves evaluating the combined score's ability to predict peritoneal recurrence-free survival (pRFS) at 2, 3, and 5 years. **c.** Kaplan-Meier plots comparing peritoneal recurrence-free survival (pRFS; left), overall recurrence-free survival (RFS; middle), and overall survival (OS; right) between patients grouped as high or low risk according to the combined score. **d.** Box plots displaying area under the curve (AUC) comparisons between the combined score and individual predictors. *P < 0.05, **P < 0.01, ***P < 0.001, ****P < 0.0001.

Abbreviations: PM = peritoneal metastasis; pRFS = peritoneal recurrence-free survival; RFS = recurrence-free survival; OS = overall survival; HR = hazard ratio; CI = confidence interval; AUC = area under the curve.

Subgroup analysis stratified by the combined score in the SYSUCC cohort revealed that high-risk patients gained substantial advantage from adjuvant chemotherapy, achieving better pRFS (HR: 0.52, 95% CI: 0.34–0.79, P = 0.002), RFS (HR: 0.53, 95% CI: 0.35–0.80, P = 0.003), and OS (HR: 0.40, 95% CI: 0.26–0.62, P < 0.001). By contrast, low-risk patients derived no

meaningful survival improvement from adjuvant chemotherapy across these endpoints **(Figure 4).**

Applying the same strategy to the TCGA cohort, we created a distinct combined score that integrated the PM risk score with age and pathologic N stage **(Table 5, Figure 3a).** This score reliably forecasted survival outcomes (5-year OS AUC: 0.79, 95% CI: 0.71–0.88), though it did not match the predictive strength of the SYSUCC-derived combined score **(Figures 3b-d).**

CASC15 facilitates gastric cancer metastasis in vitro and in vivo

To elucidate how the identified long non-coding RNAs (lncRNAs) influence peritoneal metastasis and patient outcomes, we prioritized candidates showing the largest hazard ratios. Two lncRNAs, RP11-426C22.4 and CTD-2227E11.1, lacked significant survival associations and were excluded. Between the remaining candidates—RP11-400N13.3 and CASC15—we selected CASC15 for detailed functional studies because it had the greater regression coefficient in the LASSO model.

Real-time quantitative PCR confirmed differential CASC15 expression in various gastric cancer cell lines compared with the normal gastric epithelial cell line GES-1 **(Figure 5a).** We established and validated stable cell models with either reduced or elevated CASC15 expression **(Figure 5b).**

In functional experiments, reducing CASC15 levels markedly impaired gastric cancer cell migration and invasion, as shown in wound-healing assays, Transwell chambers, and 3D tumor spheroid invasion models **(Figures 5a-e**; all $P < 0.05$). Overexpressing CASC15, however, strongly enhanced these metastatic behaviors **(Figures 5f-h**; all $P < 0.05$). Cell proliferation was also modulated by CASC15, as demonstrated by CCK-8 and colony-formation assays **(Figures 5c-e).**

Importantly, CASC15 suppression increased cellular sensitivity to frontline gastric cancer chemotherapeutics, 5-fluorouracil (5-FU) and oxaliplatin **(Figures 5f-g).** This laboratory observation mirrors the clinical finding that high-combined-score patients in the SYSUCC cohort experienced significant benefit from adjuvant chemotherapy **(Figure 4).**

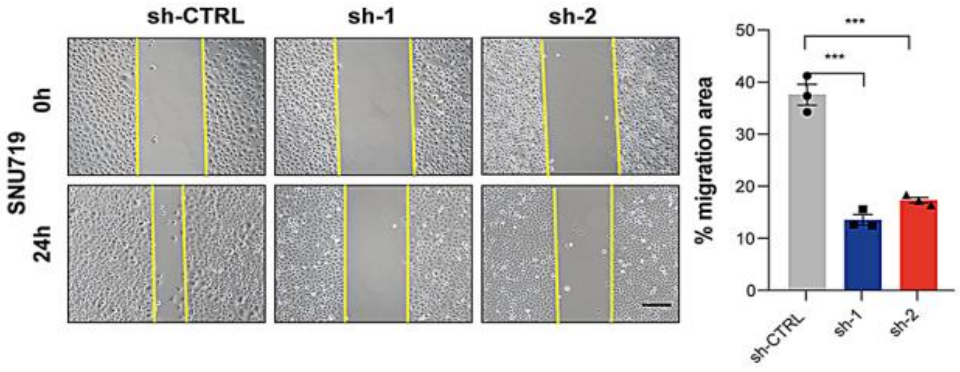

a)

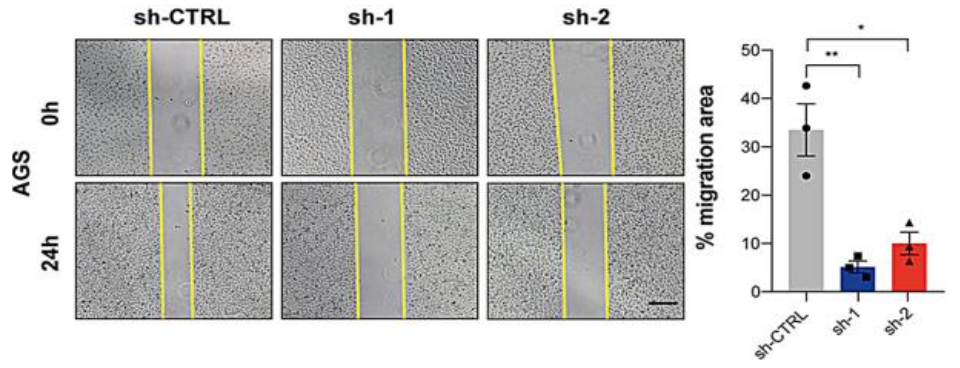

b)

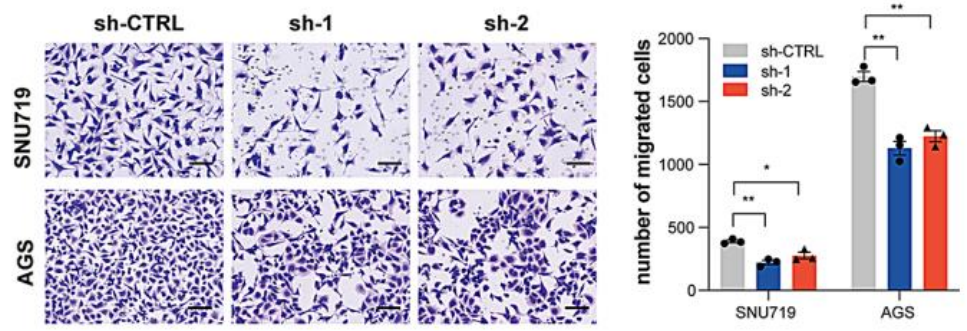
sh-CTRL
sh-1
sh-2
SNU719
AGS
number of migrated cells
2000
1500
1000
500
0
sh-CTRL
sh-1
sh-2
SNU719
AGS

c)

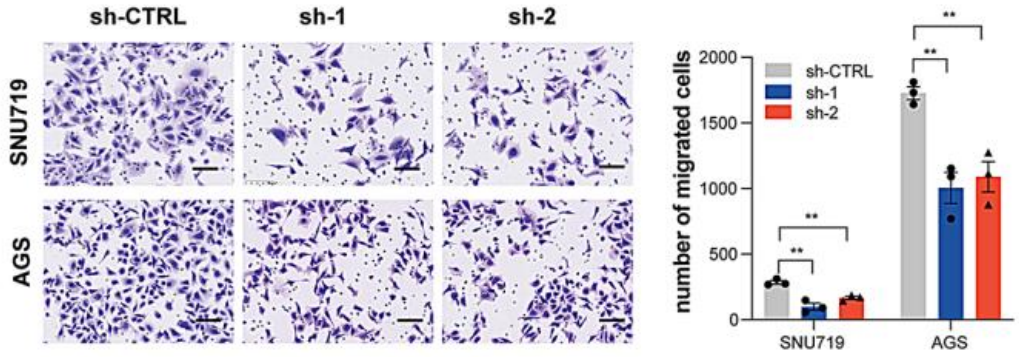
sh-CTRL
sh-1
sh-2
SNU719
AGS
number of migrated cells
2000
1500
1000
500
0
sh-CTRL
sh-1
sh-2
SNU719
AGS

d)

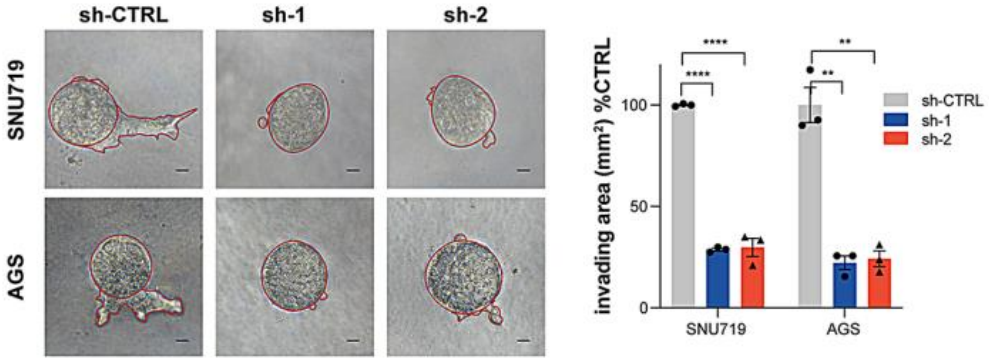
sh-CTRL
sh-1
sh-2
SNU719
AGS
invading area (mm²) %CTRL
100
50
0
sh-CTRL
sh-1
sh-2
SNU719
AGS

e)

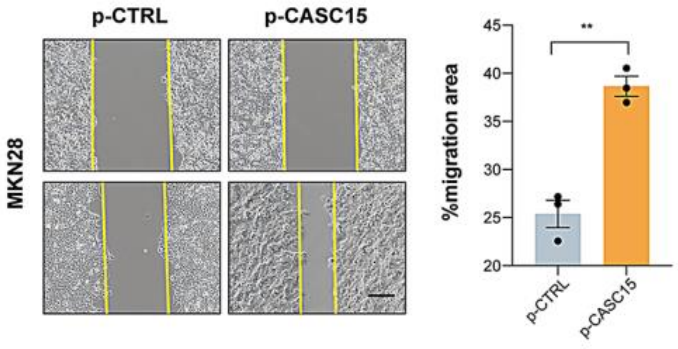
p-CTRL
p-CASC15
MKN28
%migration area
45
40
35
30
25
20
p-CTRL
p-CASC15

f)

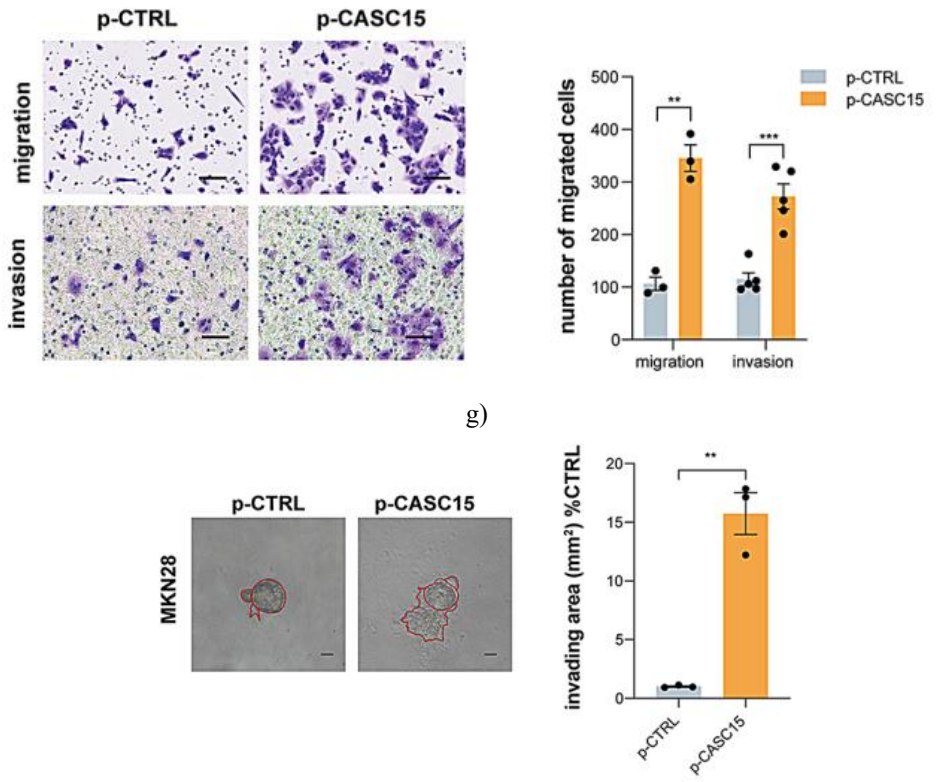

Figure 5. CASC15 drives gastric cancer cell metastasis in vitro

a–b. Scratch-wound assays testing how reduced CASC15 expression impacts the movement of specific gastric cancer cell lines. Left: example micrographs. Right: bar charts quantifying the migrated distance as a percentage. Scale bar: 200 μm. **c–d.** Transwell chamber experiments exploring the role of CASC15 downregulation in cell migration (c) and matrix invasion (d) for the chosen gastric cancer cells. Left: typical images. Scale bar: 100 μm. Right: bar charts counting migrated or invaded cells. **e.** 3D tumor spheroid invasion model assessing whether lowering CASC15 levels affects invasive growth in selected gastric cancer cells. Left: example images. Scale bar: 20 μm. Right: bar graph of invasion extent, expressed relative to the central spheroid in controls. **f.** Scratch-wound assay examining the consequences of increased CASC15 expression on cell movement in particular gastric cancer lines. Left: representative micrographs. Right: bar chart of migrated area percentage. Scale bar: 200 μm. **g.** Transwell experiments evaluating how elevated CASC15 influences migration (top) and invasion (bottom) in the specified gastric cancer cells. Left: typical images. Scale bar: 100 μm. Right: bar charts tallying migrated and invaded cells. **h.** 3D spheroid invasion assay investigating the impact of CASC15 upregulation on invasive properties in chosen gastric cancer cells. Left: example images. Scale bar: 20 μm. Right: bar graph displaying the invasion-to-core ratio, normalized against controls. Red outline marks the core spheroid and surrounding invasive zone. Across panels **a–h**, results are shown as mean ± SEM, with scatter points indicating replicates from separate experiments. Comparisons used two-tailed unpaired Student's t-tests. Raw data are included in the Source Data file. *$P < 0.05$, **$P < 0.01$, ***$P < 0.001$, ****$P < 0.0001$.

To examine whether CASC15 contributes to peritoneal metastasis of gastric cancer in living organisms, we generated peritoneal xenograft models by injecting modified gastric cancer cells into the abdominal cavity of Balb/c nude mice and NOG mice. Tumor development was followed longitudinally with a live-animal bioluminescence imaging platform (IVIS). Imaging data indicated substantially fewer peritoneal tumors when CASC15 was silenced, whereas forcing its expression increased tumor burden (**Figures 6a–e**, $P < 0.05$). At termination (3–4 weeks), direct enumeration of visible

abdominal nodules corroborated these imaging results (**Figure 6**, $P < 0.05$).

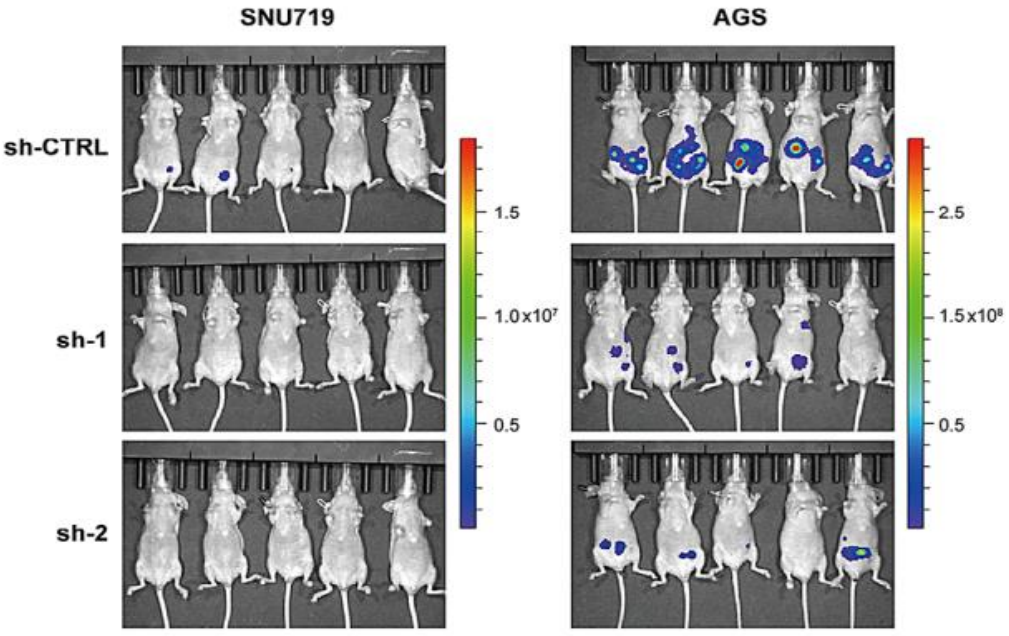

a)

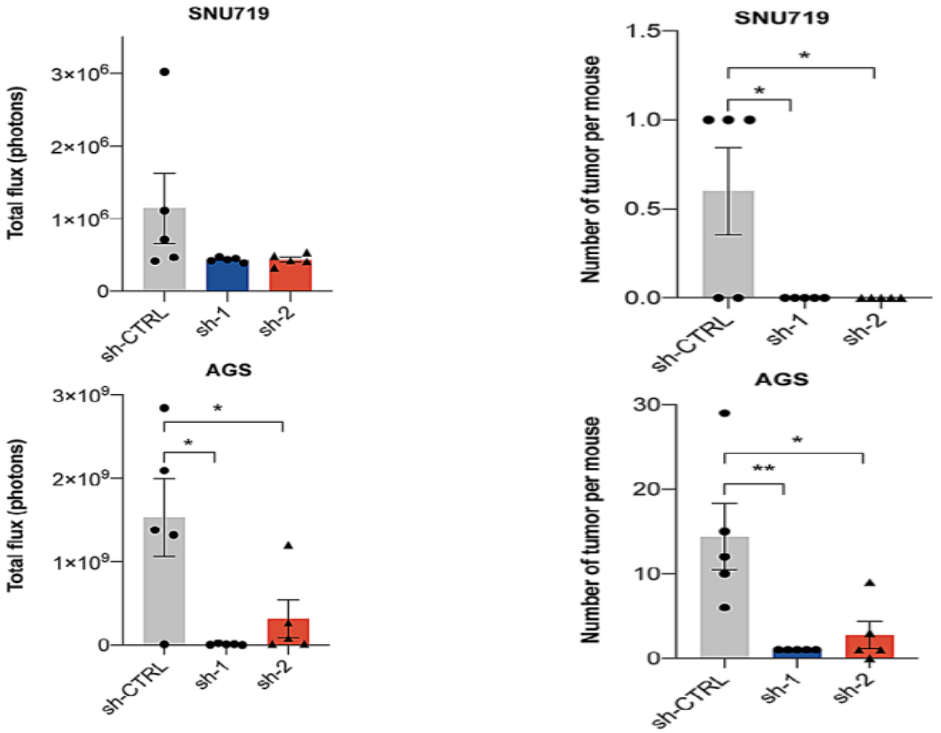

b)

c)

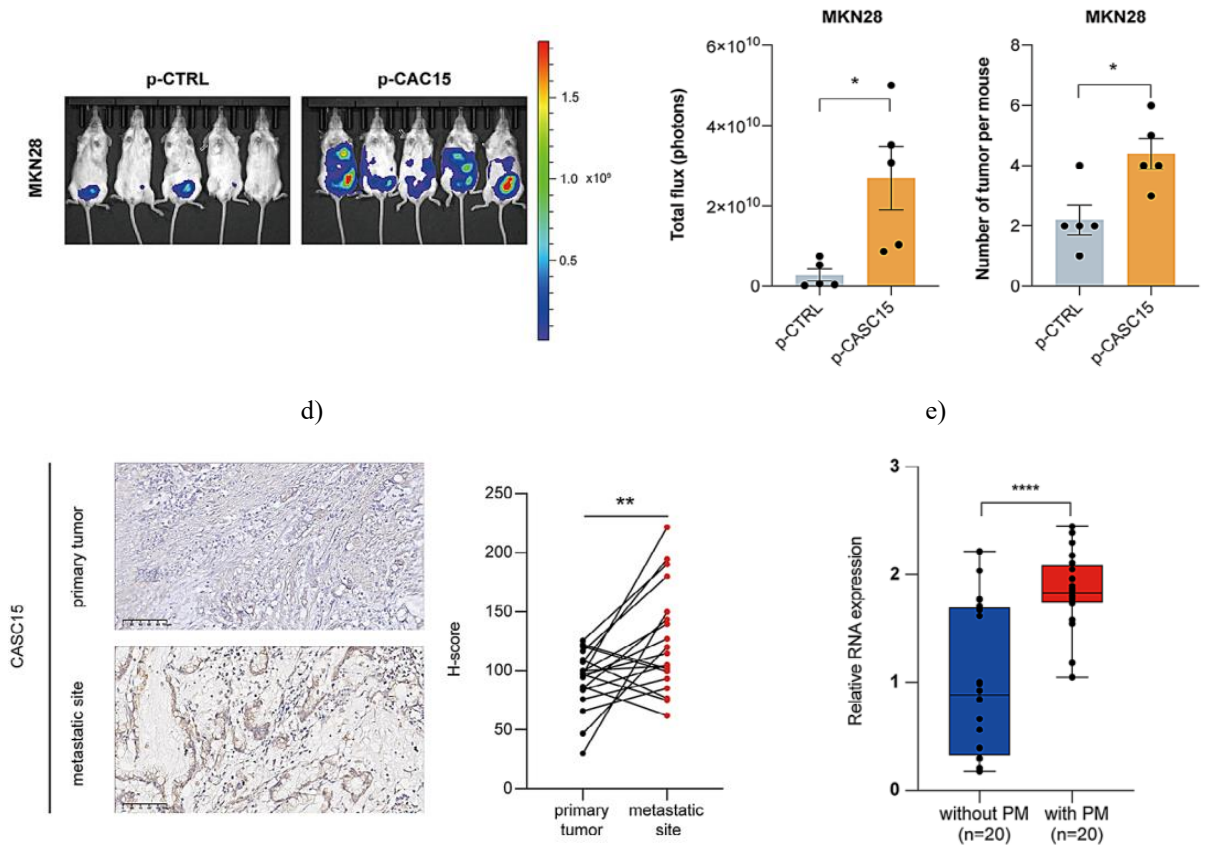

Figure 6. CASC15 enhances peritoneal metastasis of gastric cancer (GC) cells in vivo. **(a–c)** The influence of CASC15 knockdown on tumor formation was evaluated using IVIS imaging in the indicated GC cells (n = 5 mice). **(a)** Shows representative bioluminescence images for each group at weeks 3 and 4. **(b)** Quantification of luminescent signal intensity. **(c)** Number of tumors per mouse, determined by counting xenografts from the abdominal cavity post-dissection. **(d–e)** IVIS imaging assessing the effect of CASC15 overexpression on tumorigenicity in GC cells (n = 5 mice). **(d)** Representative images at week 4. **(e)** Left panel: luminescence intensity; right panel: tumor counts per mouse, assessed as above. **(f)** In situ hybridization analysis of CASC15 in primary tumors and matched metastatic lesions from patients with peritoneal metastasis. Left: representative images (scale bar, 100 μm). Right: H-score comparison. **(G)** Plasma levels of CASC15 in patients with or without peritoneal metastases are shown as a boxplot. For **(a–e)**, data are presented as mean ± SEM, with dots representing individual mice; comparisons were made using a two-tailed unpaired Student's t-test. For **(f)**, paired tissues are connected, and a paired t-test was used. For **(g)**, data are shown as min–max with statistical evaluation via Wilcoxon test.

*Source data are included in the Source Data file. *P < 0.05, **P < 0.01, ***P < 0.001, ****P < 0.0001, ns = not significant.

To validate these findings in patient samples, GC tissues from 19 individuals with peritoneal metastasis, including both primary tumors and metastatic lesions, were examined for CASC15 expression. CASC15 was consistently higher in metastatic sites than in primary tumors, confirming its role in promoting metastasis **(Figure 6f).** Plasma analysis of 40 patients further showed elevated CASC15 in those with peritoneal metastasis, suggesting it could serve as a biomarker for PM risk (**Figure 6g**, P < 0.05).

CASC15 drives GC metastasis via p38 and JNK pathways

To explore the mechanism of CASC15 in metastasis, its cellular localization was assessed, revealing predominant cytoplasmic distribution in GC cells (**Figure 7a**). Transcriptome profiling of SNU719 cells with stable CASC15 knockdown versus controls was performed. KEGG and GO analyses of downregulated genes revealed enrichment in EMT-related processes, such as extracellular matrix organization, wound healing, focal adhesion, and cell-substrate junction formation **(Figures 7b and 7a).**

Protein and transcriptional analysis showed that CASC15 knockdown decreased N-cadherin, Vimentin, and α-smooth muscle actin, while E-cadherin and β-catenin increased. Conversely, overexpression of CASC15 induced the opposite pattern **(Figures 7c–d and 7b),** and transcriptional changes matched protein expression **(Figure.7c).** Additionally, pseudopodia formation was reduced with CASC15 knockdown but enhanced upon overexpression (**Figure 7d**). These results indicate that CASC15 promotes GC metastasis by facilitating EMT.

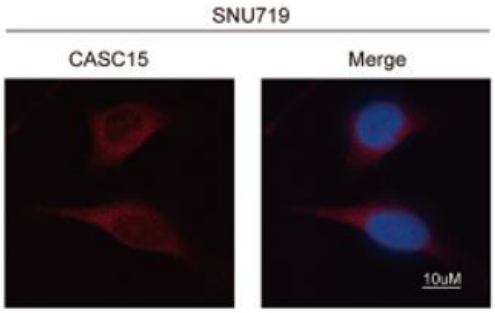

a)

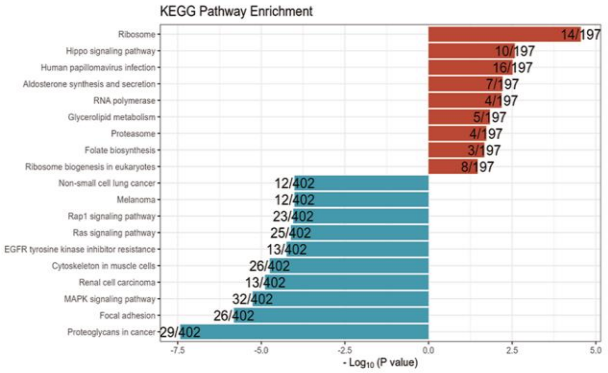

b)

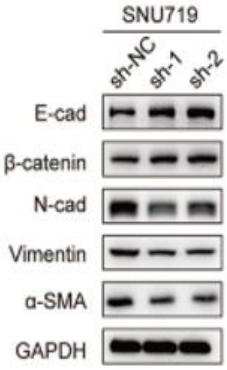

c)

d)

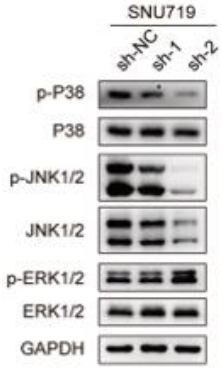

e)

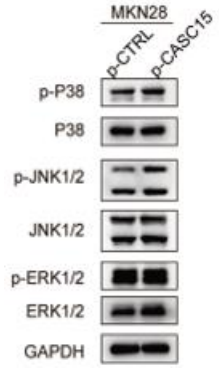

f)

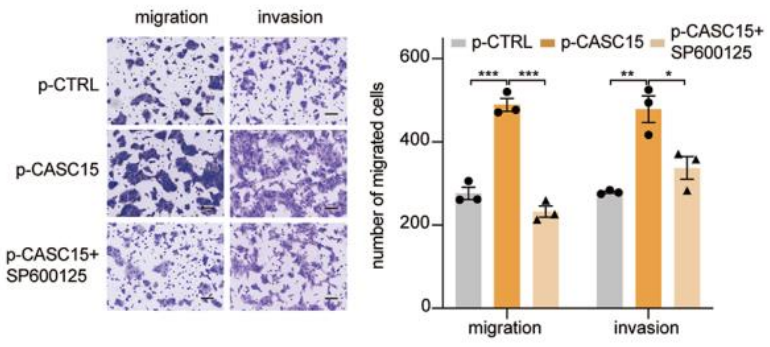

g)

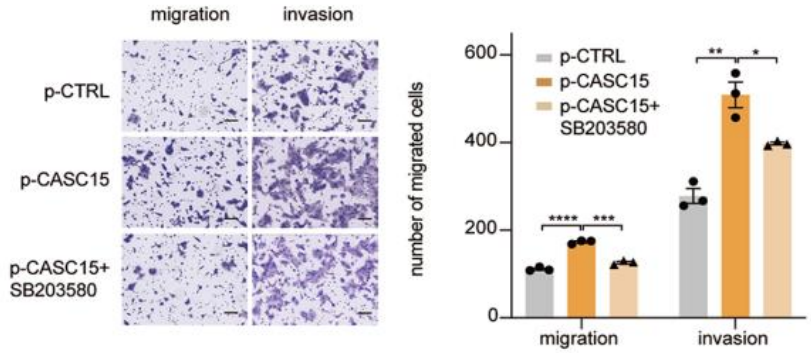

h)

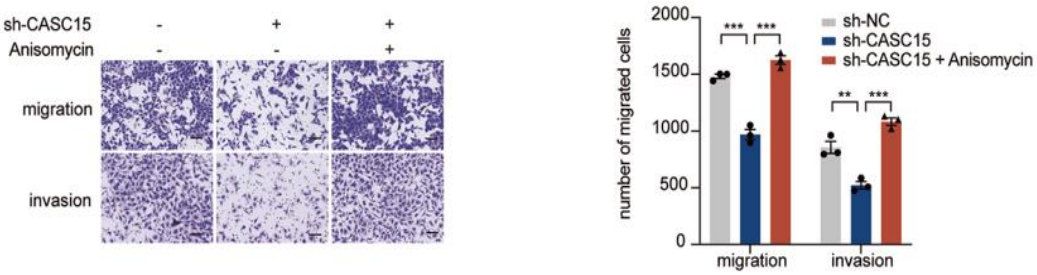

i)

Figure 7. CASC15 facilitates gastric cancer metastasis through activation of p38 and JNK pathways

a**.** RNA immuno-FISH assay determining the subcellular distribution of CASC15 in gastric cancer cells. b**.** KEGG pathway enrichment analysis highlighting significantly affected pathways based on differentially expressed mRNAs in CASC15-knockdown gastric cancer cells versus controls. c–d**.** Western blot analysis illustrating the impact of CASC15 knockdown (c) and overexpression (d) on protein levels associated with the epithelial-mesenchymal transition (EMT) process. e–f**.** Western blot results showing how CASC15 knockdown (e) and overexpression (f) alter the expression of critical proteins in the MAPK signaling cascade. g–h**.** Transwell experiments revealing that treatment with the JNK inhibitor SP600125 (20 μM for 24 h) and the p38 inhibitor SB203580 (15 μM for 24 h) partially blocks the enhanced migration and invasion induced by CASC15 overexpression in gastric cancer cells. Left: example images. Scale bar: 100 μm. Right: bar graphs quantifying migrated and invaded cell counts. i**.** Transwell experiments demonstrating that the JNK/p38 activator anisomycin (100 nM for 12 h) rescues the reduced migration and invasion seen in CASC15-knockdown gastric cancer cells. Left: example images. Scale bar: 100 μm. Right: bar graphs quantifying migrated and invaded cell counts. For panels g–i, results are expressed as mean ± SEM from three separate experiments, with individual data points shown in dot plots. Differences were evaluated using two-tailed unpaired Student's t-tests. Source data are available in the Source Data file. $^{*}P < 0.05$, $^{**}P < 0.01$, $^{***}P < 0.001$, $^{****}P < 0.0001$.

Enrichment analysis of genes downregulated following CASC15 knockdown prominently featured the MAPK signaling pathway. To determine whether this pathway mediates CASC15's effects, we examined key components and observed marked reductions in phosphorylated JNK (p-JNK) and phosphorylated p38 (p-p38) in knockdown cells, with the opposite pattern in cells overexpressing CASC15 **(Figures. 7e–f and 7e).**

To establish the functional relevance of the p38 and JNK branches in CASC15-driven gastric cancer progression, we performed rescue studies. Application of the JNK inhibitor SP600125 and the p38 inhibitor SB203580 noticeably diminished the heightened migratory and invasive abilities conferred by CASC15 overexpression **(Figures 7g–h).** Conversely, activating JNK and p38 with anisomycin effectively restored migration and invasion in CASC15-depleted cells **(Figure 7i).** Collectively, these findings indicate that CASC15 promotes gastric cancer metastasis largely through activation of the JNK and p38 signaling pathways.

Long non-coding RNAs (lncRNAs) serve as important biomarkers owing to their unique expression profiles in various normal and disease states, providing valuable information for disease diagnosis and prognostic evaluation [19]. These molecules often display tissue-specific and disease-specific characteristics, allowing for more targeted and accurate identification [20]. Furthermore, their robustness in circulation and ease of detection in multiple biofluids and tissues make them promising for biomarker development and potential therapeutic targets [21].

In the present work, we investigated the utility of lncRNAs in detecting peritoneal metastasis (PM) in gastric cancer (GC). We performed comprehensive lncRNA transcriptome profiling using paired samples from peritoneal metastases, primary gastric tumors, and adjacent normal gastric mucosa obtained from 12 GC patients in the Sun Yat-sen University Cancer Center (SYSUCC) discovery cohort. Through integrated analysis with data from The Cancer Genome Atlas (TCGA), we pinpointed 10 critical lncRNAs. Subsequent cross-validation and least absolute shrinkage and selection operator (LASSO) regression in the SYSUCC validation cohort narrowed this down to five key candidates. Based on these, we established a PM risk score capable of forecasting peritoneal recurrence-free survival (pRFS), with elevated scores correlating with increased likelihood of peritoneal relapse.

We then developed an enhanced integrated nomogram that combined the PM risk score with pathologic T stage (pT), pathologic N stage (pN), and tumor size. This composite score reliably predicted pRFS, overall recurrence-free survival (RFS), and overall survival (OS) in GC patients following curative gastrectomy, while also markedly improving the ability to identify those likely to benefit from adjuvant chemotherapy.

In addition, we delved deeper into one prominent lncRNA, CASC15, and showed that it drives GC cell metastasis in vitro and promotes peritoneal dissemination in vivo. We further provided preliminary evidence that CASC15 accelerates the epithelial-mesenchymal transition (EMT) by activating the JNK and p38 MAPK signaling cascades, thereby facilitating gastric cancer progression. Overall, this research offers early support for the contribution of lncRNAs to PM in GC. To advance clinical translation, we created an lncRNA-derived integrated score for individualized forecasting of peritoneal recurrence. Additionally, CASC15 emerges as a promising candidate for non-invasive liquid biopsy-based detection of PM in GC.

Peritoneal metastasis remains a major obstacle in the clinical handling of GC and represents the most common recurrence mode following curative resection [2, 5, 22]. However, reliable strategies for identifying postoperative peritoneal recurrence are still lacking, largely because physiological alterations in peritoneal tissues complicate accurate diagnosis. Conventional imaging modalities have inherent shortcomings in this setting. Prior efforts include a transcriptomic signature developed by Lee for risk stratification and detection of patients at high risk for peritoneal carcinomatosis [23], an miRNA-based panel proposed by Shimura for recognizing PM in GC [24], and a collagen-related nomogram constructed by Chen to estimate PM risk in serosa-invasive GC after radical surgery [25]. Despite these advances, none has achieved widespread clinical adoption.

Our work introduces an alternative lncRNA-focused predictive model derived from whole-transcriptome data, which we merged with standard clinicopathologic variables to generate a more robust integrated score. This tool not only forecasts peritoneal recurrence but also extends to overall recurrence and survival outcomes. The broader predictive scope likely reflects the dominance of peritoneal failure as the primary recurrence pattern and a leading cause of death in GC patients.

Synchronous PM refers to peritoneal involvement diagnosed concurrently with the primary GC or during planned curative surgery, whereas metachronous PM denotes peritoneal recurrence identified after successful radical resection. Our investigation began by examining synchronous PM cases to map the lncRNA expression landscape and isolate key candidates. This design was advantageous because synchronous cases readily provide matched primary tumor, metastatic, and normal tissues without prior therapeutic interference, yielding cleaner and more convincing sequencing data. Supporting this strategy, Teng and colleagues identified overlapping differentially expressed proteins between synchronous and metachronous PM, suggesting shared mechanistic drivers [26]. Accordingly, we built our predictive model using synchronous PM data and successfully demonstrated its effectiveness in anticipating metachronous peritoneal recurrence. Of note, plasma levels of CASC15 were elevated in patients with PM compared to those without, implying that CASC15 may serve as a marker for both synchronous and

metachronous disease and highlighting its wide potential utility.

Standard guidelines endorse adjuvant chemotherapy for pathologic stage II and III GC [7, 27], yet benefit is uneven across patients [28], especially in those with deficient mismatch repair (dMMR) or high microsatellite instability (MSI-H) [29]. More refined patient selection is needed to spare non-responders from treatment toxicity and costs. Here, we found that individuals with high integrated scores gained substantial survival advantages from adjuvant chemotherapy, while those with low scores showed no improvement. Consistent with this, CASC15 depletion heightened GC cell responsiveness to standard agents like 5-fluorouracil (5-FU) and oxaliplatin. These observations position the integrated score as a useful postoperative decision aid and raise the possibility that CASC15 inhibitors could enhance chemosensitivity. Nonetheless, the modest cohort size introduces potential bias, warranting confirmation in larger multicenter trials.

Conceptually, lncRNAs can influence PM risk in GC by directly regulating metastatic cascades. Earlier reports link lncRNAs to PM promotion or suppression via mechanisms such as ferroptosis [30] and fatty acid metabolic rewiring [31]. We chose CASC15 as an exemplar for mechanistic scrutiny and confirmed its capacity to boost GC cell migration and invasion in vitro, as well as peritoneal seeding in vivo. Its pro-metastatic effects rely on activation of JNK and p38 signaling. These insights bolster the rationale for using lncRNAs as PM predictors in GC.

Certain limitations should be acknowledged. The TCGA dataset lacked detailed recurrence timing and patterns, preventing full external validation of the score. Although our lncRNA model effectively forecasts both synchronous and metachronous PM, independent confirmation from other centers is essential. Moreover, calculating the score currently requires invasive tumor sampling. Encouragingly, our preliminary data support CASC15 detection in plasma as a non-invasive PM indicator. Future efforts will include expanded cohorts to rigorously test this liquid biopsy approach.

Conclusion

In conclusion, this study characterized the transcriptional profile of gastric cancer and established an integrated lncRNA-based score that enables individualized prediction of peritoneal recurrence and overall survival. Additionally, this score effectively identifies patients most likely to benefit from adjuvant chemotherapy, supporting more precise and tailored treatment planning.

Acknowledgments: None

Conflict of Interest: None

Financial Support: This research was supported by the National Natural Science Foundation of China (82103586, to RCN), Guangdong Basic and Applied Basic Research Foundation (2022A1515012458, to YFL), and Beijing Xisike Clinical Oncology Research Foundation (Y-2022METAZMS-0123, to YFL; Y-HR2022MS-0324, to SQY). The funders played no role in the study's design, conduct, or reporting.

Ethics Statement: This study was conducted in accordance with the Declaration of Helsinki. The study was approved by the Institutional Review Board (IRB) of Sun Yat-Sen University Cancer Center (SYSUCC, Guangzhou, China) with the IRB number of G2021-036.

References

1. Sung H, Ferlay J, Siegel RL, et al. Global Cancer statistics 2020: GLOBOCAN estimates of incidence and Mortality Worldwide for 36 cancers in 185 countries. CA Cancer J Clin. 2021;71(3):209–49. [published Online First: 2021/02/05].
2. Yoo CH, Noh SH, Shin DW, et al. Recurrence following curative resection for gastric carcinoma. Br J Surg. 2000;87(2):236–42.
3. Sasako M, Sano T, Yamamoto S, et al. D2 lymphadenectomy alone or with para-aortic nodal dissection for gastric cancer. N Engl J Med. 2008;359(5):453–62. 10.1056/NEJMoa0707035.
4. Fujitani K, Yang H-K, Mizusawa J, et al. Gastrectomy plus chemotherapy versus chemotherapy alone for advanced gastric cancer with a single non-curable factor (REGATTA): a phase 3, randomised controlled trial. Lancet Oncol. 2016;17(3):309–18. 10.1016/S1470-2045(15)00553-7.
5. Thomassen I, van Gestel YR, van Ramshorst B, et al. Peritoneal carcinomatosis of gastric origin: a population-based study on incidence, survival and risk factors. Int J Cancer. 2014;134(3):622–28. 10.1002/ijc.28373.

6. Burbidge S, Mahady K, Naik K. The role of CT and staging laparoscopy in the staging of gastric cancer. Clin Radiol. 2013;68(3):251–55. 10.1016/j.crad.2012.07.015.
7. Wang F-H, Zhang X-T, Tang L, et al. The Chinese Society of Clinical Oncology (CSCO): clinical guidelines for the diagnosis and treatment of gastric cancer, 2023. Cancer Commun (London England). 2024;44(1):127–72. 10.1002/cac2.12516.
8. Dong D, Tang L, Li ZY, et al. Development and validation of an individualized nomogram to identify occult peritoneal metastasis in patients with advanced gastric cancer. Annals Oncology: Official J Eur Soc Med Oncol. 2019;30(3):431–38. 10.1093/annonc/mdz001.
9. Kim SJ, Kim H-H, Kim YH, et al. Peritoneal metastasis: detection with 16- or 64-detector row CT in patients undergoing surgery for gastric cancer. Radiology. 2009;253(2):407–15. 10.1148/radiol.2532082272.
10. Mattick JS, Amaral PP, Carninci P, et al. Long non-coding RNAs: definitions, functions, challenges and recommendations. Nat Rev Mol Cell Biol. 2023;24(6):430–47. 10.1038/s41580-022-00566-8.
11. Statello L, Guo C-J, Chen L-L, et al. Gene regulation by long non-coding RNAs and its biological functions. Nat Rev Mol Cell Biol. 2021;22(2). 10.1038/s41580-020-00315-9.
12. Ali SA, Peffers MJ, Ormseth MJ, et al. The non-coding RNA interactome in joint health and disease. Nat Rev Rheumatol. 2021;17(11):692–705. 10.1038/s41584-021-00687-y.
13. Zhou M, Bao S, Gong T, et al. The transcriptional landscape and diagnostic potential of long non-coding RNAs in esophageal squamous cell carcinoma. Nat Commun. 2023;14(1):3799. 10.1038/s41467-023-39530-1.
14. Dong C, Luan F, Tian W, et al. Identification and validation of crucial lnc-TRIM28-14 and hub genes promoting gastric cancer peritoneal metastasis. BMC Cancer. 2023;23(1):76. 10.1186/s12885-023-10544-8. [published Online First: 2023/01/24].
15. Wang S, Wo L, Zhang Z, et al. Delivery of LINC00589 via mesoporous silica nanoparticles inhibits peritoneal metastasis in gastric cancer. Cancer Lett. 2022;549:215916. 10.1016/j.canlet.2022.215916. [published Online First: 2022/09/21].
16. Chen R-X, Chen X, Xia L-P, et al. N6-methyladenosine modification of circNSUN2 facilitates cytoplasmic export and stabilizes HMGA2 to promote colorectal liver metastasis. Nat Commun. 2019;10(1):4695. 10.1038/s41467-019-12651-2.
17. He Y, Sun MM, Zhang GG, et al. Targeting PI3K/Akt signal transduction for cancer therapy. Signal Transduct Target Therapy. 2021;6(1):425. 10.1038/s41392-021-00828-5.
18. Sleeboom JJF, van Tienderen GS, Schenke-Layland K, et al. The extracellular matrix as hallmark of cancer and metastasis: from biomechanics to therapeutic targets. Sci Transl Med. 2024;16(728):eadg3840. 10.1126/scitranslmed.adg3840.
19. Nair L, Chung H, Basu U. Regulation of long non-coding RNAs and genome dynamics by the RNA surveillance machinery. Nat Rev Mol Cell Biol. 2020;21(3):123–36. 10.1038/s41580-019-0209-0.
20. Bhan A, Soleimani M, Mandal SS. Long noncoding RNA and Cancer: a New Paradigm. Cancer Res. 2017;77(15):3965–81. 10.1158/0008-5472.CAN-16-2634.
21. Badowski C, He B, Garmire LX. Blood-derived lncRNAs as biomarkers for cancer diagnosis: the Good, the bad and the Beauty. NPJ Precis Oncol. 2022;6(1):40. 10.1038/s41698-022-00283-7.
22. Lu J, Xu B-B, Zheng H-L, et al. Robotic versus laparoscopic distal gastrectomy for resectable gastric cancer: a randomized phase 2 trial. Nat Commun. 2024;15(1):4668. 10.1038/s41467-024-49013-6.
23. Lee I-S, Lee H, Hur H, et al. Transcriptomic profiling identifies a risk stratification signature for Predicting Peritoneal recurrence and Micrometastasis in Gastric Cancer. Clin Cancer Research: Official J Am Association Cancer Res. 2021;27(8):2292–300. 10.1158/1078-0432.CCR-20-3835.
24. Shimura T, Toden S, Kandimalla R, et al. Genomewide expression profiling identifies a Novel miRNA-based Signature for the detection of peritoneal metastasis in patients with gastric Cancer. Ann Surg. 2021;274(5):e425–34. 10.1097/SLA.0000000000003647.
25. Chen D, Liu Z, Liu W, et al. Predicting postoperative peritoneal metastasis in gastric cancer with serosal invasion using a collagen nomogram. Nat Commun. 2021;12(1):179. 10.1038/s41467-020-20429-0.

26. Chen Y, Cai G, Jiang J, et al. Proteomic profiling of gastric cancer with peritoneal metastasis identifies a protein signature associated with immune microenvironment and patient outcome. Gastric Cancer: Official J Int Gastric Cancer Association Japanese Gastric Cancer Association. 2023;26(4):504–16. 10.1007/s10120-023-01379-0.
27. Sasako M, Sakuramoto S, Katai H, et al. Five-year outcomes of a randomized phase III trial comparing adjuvant chemotherapy with S-1 versus surgery alone in stage II or III gastric cancer. J Clin Oncology: Official J Am Soc Clin Oncol. 2011;29(33):4387–93. 10.1200/JCO.2011.36.5908.
28. Strickland MR, Lander EM, Gibson MK, et al. Gastroesophageal adenocarcinomas with defective mismatch repair: current knowledge and clinical management. J Natl Compr Canc Netw. 2024;22(3). 10.6004/jnccn.2023.7103.
29. An JY, Kim H, Cheong JH. Microsatellite instability in sporadic gastric cancer: its prognostic role and guidance for 5-FU based chemotherapy after R0 resection. Int J Cancer. 2012;131:505–11.
30. Lin Z, Song J, Gao Y, et al. Hypoxia-induced HIF-1α/lncRNA-PMAN inhibits ferroptosis by promoting the cytoplasmic translocation of ELAVL1 in peritoneal dissemination from gastric cancer. Redox Biol. 2022;52:102312. 10.1016/j.redox.2022.102312.
31. He Q, Yang C, Xiang Z, et al. LINC00924-induced fatty acid metabolic reprogramming facilitates gastric cancer peritoneal metastasis via hnRNPC-regulated alternative splicing of Mnk2. Cell Death Dis. 2022;13(11):987. 10.1038/s41419-022-05436-x.